



HAL
open science

Anomalous metallic state in quasi-two-dimensional BaNiS₂

David Santos-Cottin, Andrea Gauzzi, Marine Verseils, Benoit Baptiste,
Gwendal Feve, Vincent Freulon, Bernard Plaçais, Michele Casula, Yannick
Klein

► **To cite this version:**

David Santos-Cottin, Andrea Gauzzi, Marine Verseils, Benoit Baptiste, Gwendal Feve, et al.. Anomalous metallic state in quasi-two-dimensional BaNiS₂. *Physical Review B*, 2016, 93 (12), pp.125120. 10.1103/PhysRevB.93.125120 . hal-01307113

HAL Id: hal-01307113

<https://hal.sorbonne-universite.fr/hal-01307113v1>

Submitted on 11 Nov 2024

HAL is a multi-disciplinary open access archive for the deposit and dissemination of scientific research documents, whether they are published or not. The documents may come from teaching and research institutions in France or abroad, or from public or private research centers.

L'archive ouverte pluridisciplinaire **HAL**, est destinée au dépôt et à la diffusion de documents scientifiques de niveau recherche, publiés ou non, émanant des établissements d'enseignement et de recherche français ou étrangers, des laboratoires publics ou privés.

Anomalous metallic state in quasi-two-dimensional BaNiS₂

David Santos-Cottin,^{1,*} Andrea Gauzzi,¹ Marine Verseils,¹ Benoit Baptiste,¹ Gwendal Feve,² Vincent Freulon,² Bernard Plaçais,² Michele Casula,¹ and Yannick Klein^{1,†}

¹*IMPMC, Sorbonne Université-UPMC, CNRS,
IRD, MNHN, 4 place Jussieu, 75252 Paris, France*

²*Laboratoire Pierre Aigrain, Ecole Normale Supérieure-PSL Research University,
CNRS, Université Pierre et Marie Curie-Sorbonne Universités,
Université Paris Diderot-Sorbonne Paris Cité,
24 rue Lhomond, 75231 Paris Cedex 05, France*

(Dated: September 14, 2018)

Abstract

We report on a systematic study of the thermodynamic, electronic and charge transport properties of high-quality single crystals of BaNiS₂, the metallic end-member of the quasi-twodimensional BaCo_{1-x}Ni_xS₂ system characterized by a metal-insulator transition at $x_{cr} = 0.22$. Our analysis of magnetoresistivity and specific heat data consistently suggests a picture of compensated semimetal with two hole- and one electron-bands, where electron-phonon scattering dominates charge transport and the minority holes exhibit, below ~ 100 K, a very large mobility, $\mu_h \sim 15000 \text{ cm}^2\text{V}^{-1}\text{s}^{-1}$, which is explained by a Dirac-like band. Evidence of unconventional metallic properties is given by an intriguing crossover of the resistivity from a Bloch-Grüneisen regime to a linear- T regime occurring at 2 K and by a strong linear term in the paramagnetic susceptibility above 100 K. We discuss the possibility that these anomalies reflect a departure from conventional Fermi-liquid properties in presence of short-range AF fluctuations and of a large Hund coupling.

PACS numbers: 71.38.Cn, 72.15.Eb, 72.15.Gd, 72.15.Lh

Keywords: transition metal sulfide, semimetal, BaNiS₂, magnetotransport

I. INTRODUCTION

BaNiS₂ is the metal phase precursor of the metal-insulator transition (MIT) observed at $x_{cr} = 0.22$ in the quasi-two-dimensional square-lattice BaCo_{1-x}Ni_xS₂ system, where the Ni/Co substitution level, x , controls electron doping. This MIT has attracted interest for it is associated with a competition between an insulating antiferromagnetic (AF) phase and a paramagnetic metallic one¹, similar to the case of unconventional superconductors, such as cuprate², Fe-based³ and heavy-fermions⁴. On the other hand, no superconductivity has been hitherto reported in BaCo_{1-x}Ni_xS₂. In its simple tetragonal $P4/nmm$ structure⁵ made of a checkerboard-like network of edge-sharing NiS₅ pyramids (see Fig.1), all atomic coordinates are set by symmetry in the ab -plane and the structural degrees of freedom are limited to the z -coordinates along the c -axis. Because of the absence of structural distortions concomitant to the MIT, BaCo_{1-x}Ni_xS₂ is a model system for studying the doping-controlled Mott transition in a square lattice⁶, where the electronic degrees of freedom are decoupled from those of the lattice.

In order to unveil the mechanism of the MIT, previous studies have been mostly devoted to the doping region in the vicinity of x_{cr} , whilst the precursor metallic phase BaNiS₂ remains little studied. It is the purpose of the present work to systematically investigate this phase, which should help elucidating the stability of the metallic state in the important limit of no chemical disorder ($x=1$). Open questions are the relevance of electron-electron correlations to charge localization and the possibility of unconventional topological phases that may arise from the following features of the electronic structure of BaNiS₂: (i) strong spin-orbit (SO) coupling effects leading to a large Rashba splitting, which is unexpected for a compound composed by comparatively light element⁷; (ii) a Dirac-like point at the Fermi surface. In the present work, we carried out a systematic study by means of specific heat, susceptibility and magnetoresistivity measurements on high-quality single crystals. The data give evidence of anomalous properties suggesting a quantum critical point scenario controlled by AF fluctuations and by a strong Hund coupling involving the Ni²⁺ ions.

II. METHODS

BaNiS₂ single crystals were synthesized using a conventional solid state reaction method, as described in detail elsewhere⁸. In brief, powders of barium sulfide (BaS, 99.9% purity), sulfur (99.995%) and metallic nickel (99.999%) in non-stoichiometric molar ratios Ba:Ni:S = 0.10:0.425:0.475 were finely ground and pelletized. The pellets were loaded in a graphite crucible and sealed in a quartz ampoule in vacuum at pressures of 10⁻⁵ mbar or better. Graphite was used as a catalytic matrix for oxygen, thus preventing oxidation of the reagents. The heat treatment consists of a first dwell at 300 °C for 2h followed by a second one at 1100 °C for 48h, a cooling down to 850 °C at a rate of 50 °C/h and a final quench into water. The powders were ground again and a similar heat treatment as before was applied, except the cooling rate was reduced to 1 °C/h. This second treatment leads to the formation of black platelet-like single crystals of size up to $\sim 1 \times 1 \times 0.1$ mm³ that were mechanically removed from the batch and washed with ethanol. Several single crystals were selected for the present study. Single crystal x-ray diffraction yielded structural parameters $a = b = 4.4404(6)$ Å, and $c = 8.897(2)$ Å, in agreement with previous results^{5,9}. Structural refinements carried out assuming no sulfur or nickel vacancies yielded exceptionally low reliability factors, $R_w < 0.015$, thus indicating a low amount of disorder. Refinements that include the possibility of vacancies did not improve the result and systematically converged to the stoichiometric formula.

Magnetization and specific heat measurements were carried out in a Quantum Design SQUID vibrating sample magnetometer (VSM) at a field of 1 T and in a Quantum Design physical properties measurement system (PPMS) using a $2\text{-}\tau$ relaxation method, respectively. For transport measurements, the samples were contacted with silver epoxy (Dupont 6838 conductor paste) which ensures low-resistance ohmic contacts after a heat treatment under vacuum at 250 °C overnight. The in-plane (ab) longitudinal and transverse resistances, R_{xx} and R_{xy} respectively, were measured using a AC four-probe technique in the PPMS in the bar or van der Pauw¹⁰ configurations. The out-of-plane (c -axis) resistivity was measured by employing a ring geometry of the current electrode, as described elsewhere¹¹. The in-plane resistivity of a representative single crystal was measured at very low temperatures down to 40 mK in a He³ dilution refrigerator cryostat using a lock-in detection technique.

The band structure has been calculated with the Perdew-Burke-Ernzerhof density

functional¹² augmented by a local Coulomb repulsion via the spherically symmetric Hubbard matrix with $U = 3$ eV and by a Hund coupling $J = 0.95$ eV, while the Racah parameter ratio F_4/F_2 is taken from the atomic value. We used norm-conserving pseudopotentials by treating the Ni pseudoatom as fully relativistic. The spin-orbit coupling is taken into account by using the Quantum Espresso implementation¹³, with a spinor formulation based on non-collinear two-component spin-Bloch functions^{14,15}. The self-consistent calculation has converged on a 8x8x8 Monkhorst-Pack k -points grid with a plane-waves cutoff of 120 Ry. The density of states has been computed with a non-self consistent calculation on a 16x16x16 k -points grid and the tetrahedron method¹⁶.

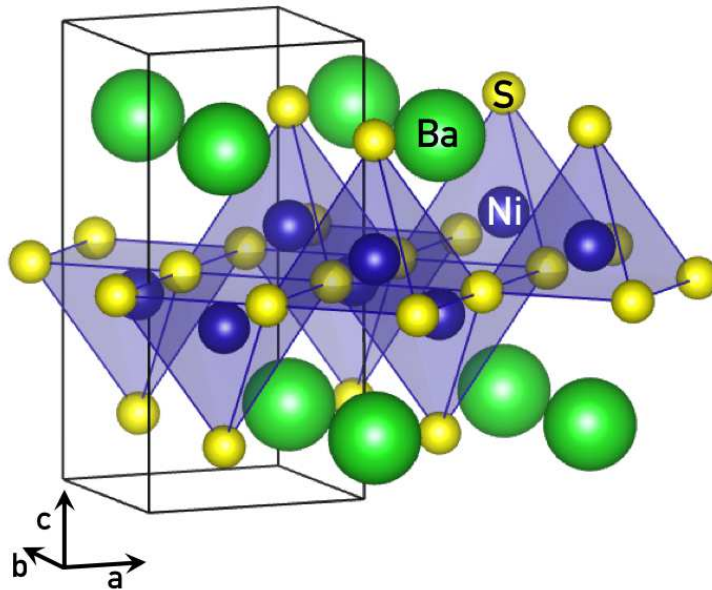


FIG. 1: (color online) Tetragonal structure of BaNiS₂. The unit cell is drawn using solid lines.

III. RESULTS

Fig. 2 shows the temperature-dependent isobaric specific heat, $C_P(T)$, measured on a bunch of single crystals of total weight 5.77 mg selected from the same batch. No anomalies are found in the whole 2-400 K range measured, which indicates the absence of phase transitions. As customary done for solids in the above range, in the present data analysis, we neglect the small difference between the *isobaric* and *isochoric* specific heats given by $C_P - C_V = \alpha^2 K_T V T$, where α , K_T and V are the thermal expansion coefficient, the isothermal bulk modulus and the molar volume, respectively. Considering the experimental value of α reported for BaNiS₂¹⁷ and typical values for K_T , the magnitude of this difference in the temperature range considered here is estimated to be $\sim 1-2\%$ or less. We then analyze the data using the usual expression for C_V that reads

$$C_V(T) = \gamma T + 9sk_B \left(\frac{T}{\theta_D}\right)^3 \int_0^{\theta_D/T} \frac{x^4 e^x}{(e^x - 1)^2} dx \quad (1)$$

where the first and second terms represent the electronic and lattice contributions, respectively, described by a conventional band model and by the Debye model. The quantities γ , s , k_B and θ_D denote the Sommerfeld coefficient, the number of atoms per mole, the Boltzmann constant and the Debye temperature, respectively. By fitting the low temperature data below 8 K, where the expression in Eq. 1 is approximated by $C_V(T)/T = \gamma + \beta T^2$ and $\beta \propto \theta_D^{-3}$, we obtain $\gamma = 2.15(11)$ mJ K⁻² mol⁻¹ and $\theta_D = 311(5)$ K. This γ value is slightly larger than previously measured on polycrystalline samples¹⁸ but comparable to the values 2.9 mJ K⁻² mol⁻¹¹⁹ and 3.1 mJ K⁻² mol⁻¹²⁰ estimated from *ab initio* DFT calculations of the density of states (DOS) at the Fermi level, $D(\epsilon_F)$, which suggests a modest mass renormalization. The extrapolation of the Debye curve to higher temperatures using the above parameters accounts for the data up to 400 K. The slight excess of the experimental value with respect to the Dulong-Petit limit $3sk_B = 99.8$ J mol⁻¹ K⁻¹ observed at such higher temperatures, is ascribed to the small difference between C_V and C_P .

In Fig. 3, we plot the DC magnetic susceptibility curves, $\chi_{ab}(T)$ and $\chi_c(T)$, in fields parallel and perpendicular to the *ab*-plane for a representative BaNiS₂ single crystal. The difference between the two curves indicates a pronounced anisotropy of the magnetic response. The averaged susceptibility is in good agreement with previous results on polycrys-

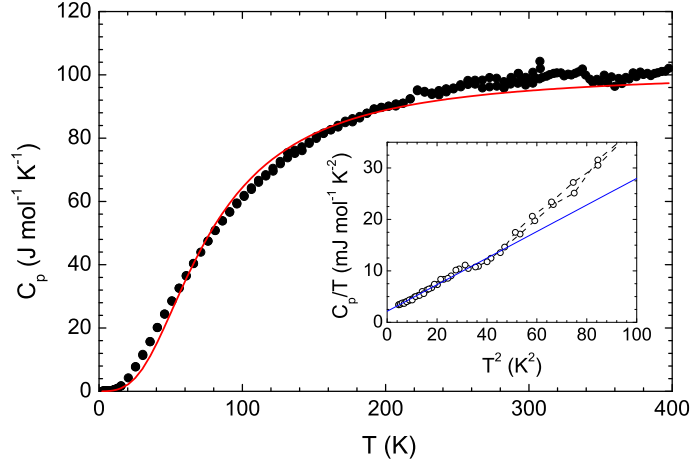


FIG. 2: (color online) Temperature dependence of the isobaric specific heat, C_P , of a bunch of BaNiS_2 single crystals. In the inset, the broken line is a fit of the low temperature data that yields γ and Θ_D . The red solid line is the theoretical Debye curve described by Eq. 1.

talline samples^{1,21,22}, except the present data show a weaker upturn at low temperature. At first sight, this may be due to a smaller concentration of paramagnetic impurities in the present single crystals. Though, no clear evidence of Curie-like behavior is found at low temperatures, so the physical origin of the upturn may be different. Notable feature of both $\chi_{ab}(T)$ and $\chi_c(T)$ is a pronounced linear behavior at high temperature with a large slope $4.2 \times 10^{-7} \text{ emu mol}^{-1} \text{ K}^{-1}$. Such behavior contrasts the expectation of a constant Pauli term in a conventional metal. A similar linear dependence with comparable slopes $\sim 4.3 \times 10^{-7} \text{ emu K}^{-1} \text{ mol}(\text{Fe})^{-1}$ and $\sim 6 \times 10^{-7} \text{ emu K}^{-1} \text{ mol}(\text{Fe})^{-1}$ has been previously reported in other semimetals, such as the parent compounds of Fe-based superconductors LaOFeAs and BaFe_2As_2 , respectively^{23,24}. For these systems, two scenarios have been proposed, one based on AF fluctuations and the other on a pronounced peak of the density of states at ϵ_F . Below, we shall discuss the suitability of these two scenarios for the present BaNiS_2 case.

Figure 4 shows the ab -plane and c -axis components of the electrical resistivity tensor, $\rho_{ab}(T)$ and $\rho_c(T)$. $\rho_{ab}(T)$ was reproducibly measured on a dozen single crystals with residual resistivity ratios $RRR = \rho_{ab}(300\text{K})/\rho_0$ ranging from 4 up to 17, where ρ_0 denotes the residual resistivity measured at 10 K (see below and inset of Fig. 4). The largest RRR 's are about 4 times larger than those previously reported⁸, which indicates a higher purity of the present

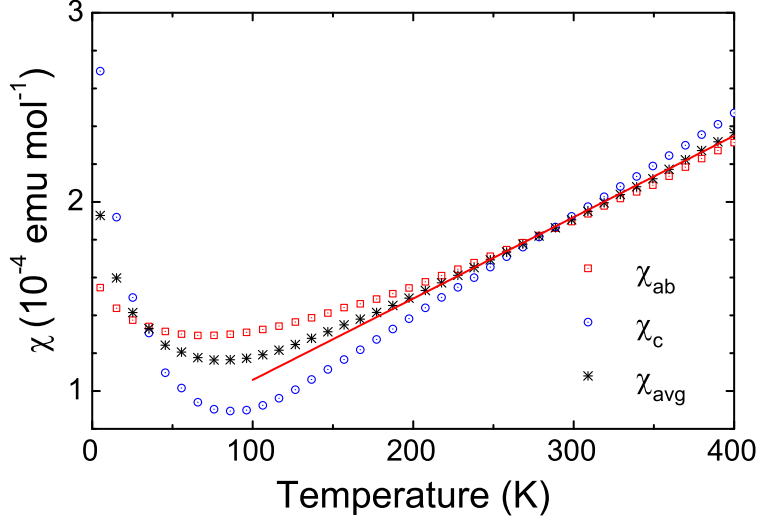


FIG. 3: (color online) Magnetic susceptibility of a BaNiS₂ single crystal. χ_{ab} and χ_c indicate the measurements taken with field in the ab -plane and along the c -axis, respectively. The average is given by $\chi_{avg} = \frac{2}{3}\chi_{ab} + \frac{1}{3}\chi_c$. The data have been corrected from the core diamagnetic susceptibility estimated to be $\chi_{core} \approx -1.2 \times 10^{-4} \text{ emu mol}^{-1}$.

crystals. The results of the present measurements confirm previous work, in particular the value of the room temperature resistivity $\rho_{ab}(300\text{K}) \approx 0.2 \text{ m}\Omega\text{cm}$, characteristic of a bad metal. ρ_{ab} and ρ_c are successfully explained by a conventional Bloch-Grüneisen model of electron-phonon scattering described by the expression:

$$\rho(T) = \rho_0 + \alpha \left(\frac{T}{\theta_D} \right)^5 \int_0^{\theta_D/T} \frac{x^5 e^x}{(e^x - 1)^2} dx \quad (2)$$

where the Eliashberg function $\alpha \sim \lambda\theta_D/\omega_p^2$, assumed to be temperature independent, depends upon the electron-phonon coupling constant, λ , and upon the plasma frequency, ω_p ²⁵. The above expression is found to account well for both ρ_{ab} and ρ_c curves up to 250 K and 200 K, respectively. A data fit yields almost identical values for the Debye temperature, $\theta_D = 330 \text{ K}$ for ρ_{ab} and $\theta_D = 332 \text{ K}$ for ρ_c . These values are in very good agreement with the $\theta_D = 311 \text{ K}$ obtained from the specific heat data, which strongly supports a picture of electron-phonon scattering. The absence of a T^2 term at low temperature indicates negligible electron-electron scattering, in agreement with the previous observation of small mass renormalization effects by means of specific heat (see above) and ARPES measurements⁷.

The anisotropy ratio is found to be $\kappa = \rho_c/\rho_{ab} \sim 8$ at 300 K and does not depend strongly on temperature and may vary in the 6-10 range from sample to sample. These values suggest quasi-two-dimensional transport properties; a more pronounced 2D character is found in unconventional metals, such as Sr_2RuO_4 ($\kappa \approx 200$), BaFe_2As_2 ($\kappa \approx 150$) and underdoped cuprates, such as $\text{YBa}_2\text{Cu}_3\text{O}_{7-\delta}$ ($\kappa \approx 100$)^{24,26,27}. Our observation of a significant contribution of the c -axis conductivity is consistent with the existence of dispersive bands along k_z ^{7,19,20}. The present result on single crystal contrasts a previous result on c -axis oriented polycrystalline samples in which much larger ratios $\kappa \sim 10^3$ were reported²¹. This discrepancy may arise from the enhanced charge scattering at grain boundaries.

Notable are the following anomalies of the temperature dependence of the resistivity:

1. At high temperature, the resistivity tends to level off.
2. In the highest purity samples, below $T^* \sim 6$ K, the in-plane resistivity does not level off at the value of the residual resistivity, ρ_0 , as in a normal metal; instead, it begins decreasing linearly with decreasing temperature down to the lowest temperature measured, 40 mK (see inset of Fig. 4a).

The possible origin of these two anomalies are discussed below.

Fig. 5 displays the longitudinal and transverse components of the resistivity, ρ_{xx} and ρ_{yx} respectively, as a function of magnetic field. A sample with $RRR = 15.8$ was chosen for this measurement. ρ_{xx} exhibits a strong variation with B which increases with decreasing temperature. The magnetoresistance $\Delta\rho_{xx}(B)/\rho_{xx}(0) = [\rho_{xx}(B) - \rho_{xx}(0)]/\rho_{xx}(0)$ does not exhibit any saturation up to 9 T and its large magnitude as high as 20 at 2 K is comparable to that of high mobility compounds, such as CuAgSe ²⁸. A large magnetoresistance is typical of compensated semimetals like Bi ²⁹, which is indeed the case of BaNiS_2 , as indicated by the aforementioned band calculations and ARPES data. The field dependence of the transverse resistivity, ρ_{yx} , is linear at high temperature, as expected, but nonlinear at low temperature. In the high RRR samples, the ρ_{yx} curve displays a change of sign, a further signature of semimetallic properties. We further analyzed the magnetoresistivity data in order to determine the carrier density and carrier mobility. The plot of Fig. 6 put into evidence a deviation from Kohler's rule³⁰, which predicts a scaling of the $\Delta\rho_{xx}(B)/\rho_{xx}(0)$ curves as a function of the scaling variable $B/\rho_{xx}(0)$. This deviation is explained by the presence of at

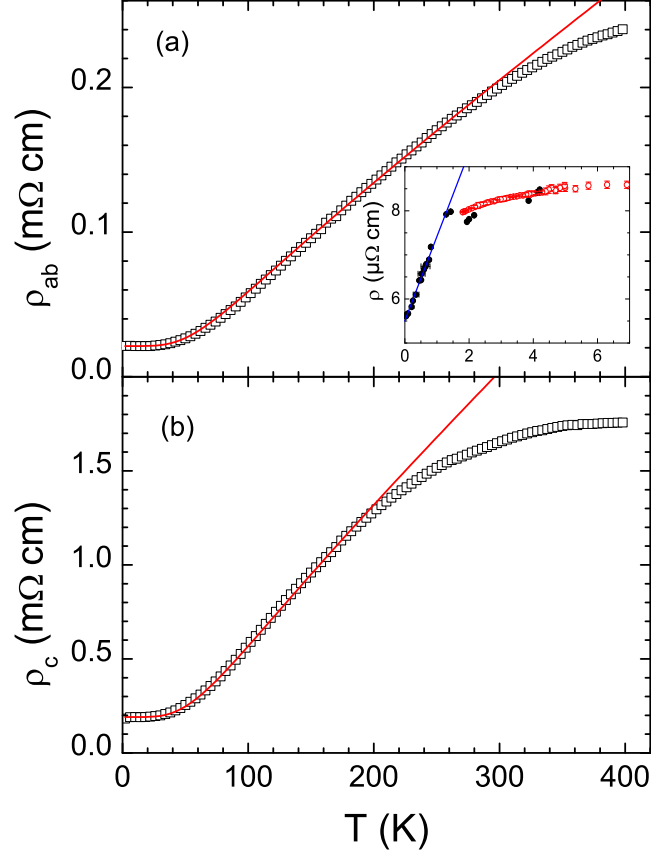


FIG. 4: ab -plane (a) and c -axis (b) resistivity of a representative BaNiS_2 single crystal with $RRR = 9.4$. The red lines are a data fit using eq. (2). The inset shows the low temperature resistivity curve obtained on a sample with $RRR=15.8$. Black and red circles indicate data obtained in a dilution cryostat and in a PPMS, respectively. The blue line is a linear fit $\rho = \rho'_0 + AT$ with $A = 1.91 \times 10^{-3} \text{ m}\Omega\text{cm K}^{-1}$ and $\rho'_0 = 5.5 \times 10^{-3} \text{ m}\Omega\text{cm}$.

least two kinds of carriers with different mobilities. To investigate this point, we analyzed the temperature and field dependent data using the usual expressions for the longitudinal and tranverse magnetoconductivity:

$$\sigma_{xx} = \sum_i \frac{|q_i| n_i \mu_i}{1 + (\mu_i B)^2} \quad (3)$$

$$\sigma_{xy} = \sum_i \frac{q_i n_i \mu_i^2 B}{1 + (\mu_i B)^2} \quad (4)$$

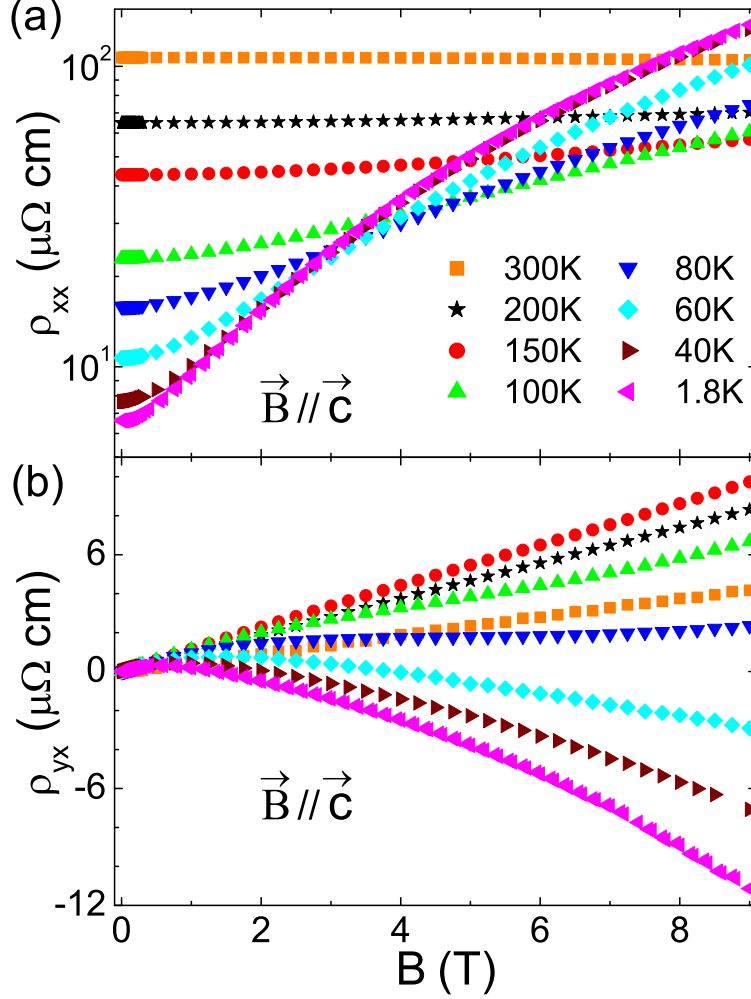


FIG. 5: (a) Transverse and (b) longitudinal magnetoresistivity of a BaNiS₂ single crystal with RRR = 15.8 at temperatures ranging from 1.8 K to 300 K. The magnetic field was applied perpendicular to the current.

where q_i , n_i and μ_i are the charge, density and mobility of the carriers and i is the band index. According to the above expressions, a significant field dependence of the conductivity appears if the term $\mu_i B$ is of the order of unity or larger. In this case, a simultaneous fit of the two components of the conductivity tensor by Eqs. (3) and (4) is possible, which allows a determination of n_i and μ_i for each band. This is indeed our case, as the curves of Fig. 7 exhibit a strong field dependence up to 100 K. In this temperature range, we then tried to determine both n_i and μ_i for each band i by using Eqs. 3 and 4. Whilst this analysis was not possible using a simple two-band model with one hole (h) and one electron

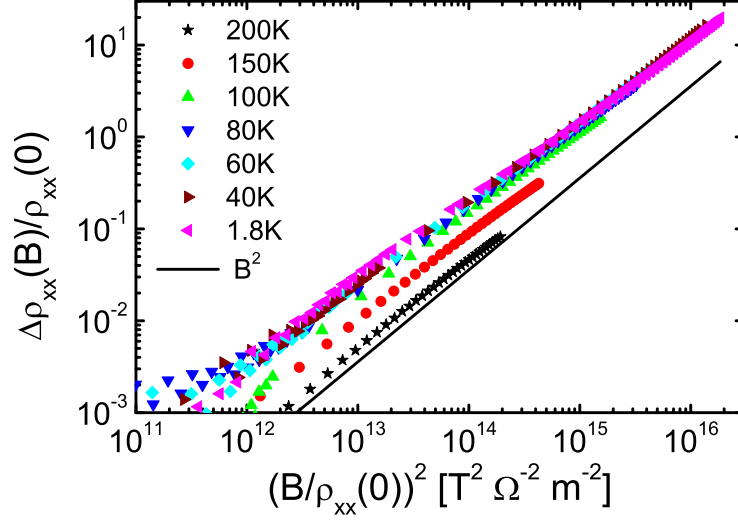


FIG. 6: Magnetoresistance $\Delta\rho/\rho(B=0)$ plotted as a function of $B^2/\rho^2(B=0)$. Note the deviation from the Kohler's rule at high temperature.

(*e*) band, the inclusion of an additional hole-band yields a very good agreement with the data, as apparent from Fig. 7. The fitting could not be extended to the data above 100 K, where the field-dependence of the magnetoconductivity is weak. The results of the data analysis are summarized in Table I. An indication of the reliability of this 3-band model is indicated by the fact that the inclusion of an extra electron - instead of hole - band was not successful. The carrier densities obtained from the above analysis are temperature and sample independent and fall in the typical $10^{19} - 10^{20} \text{ cm}^{-3}$ range for semimetals, which account for the bad metallic properties of the compound. We find an excess of electrons of $\sim 1\%$ of the total number of carriers, which confirms the picture of compensated semimetal suggested by band calculations. In Fig. 8, the mobility of the three types of carriers are plotted as a function of temperature. While electrons and type-1 (h_1) holes exhibit relatively similar mobilities, the mobility of type-2 (h_2) holes is about 4-5 times larger and reaches the remarkable value of $\sim 15000 \text{ cm}^2\text{V}^{-1}\text{s}^{-1}$ in the cleanest crystals at low temperature. These values are comparable to the values $\sim 20000 \text{ cm}^2\text{V}^{-1}\text{s}^{-1}$ reported in undoped CuAgSe²⁸ and only one order of magnitude less than in pure Si and GaAs semiconductors³¹, in spite of the much larger carrier densities in BaNiS₂.

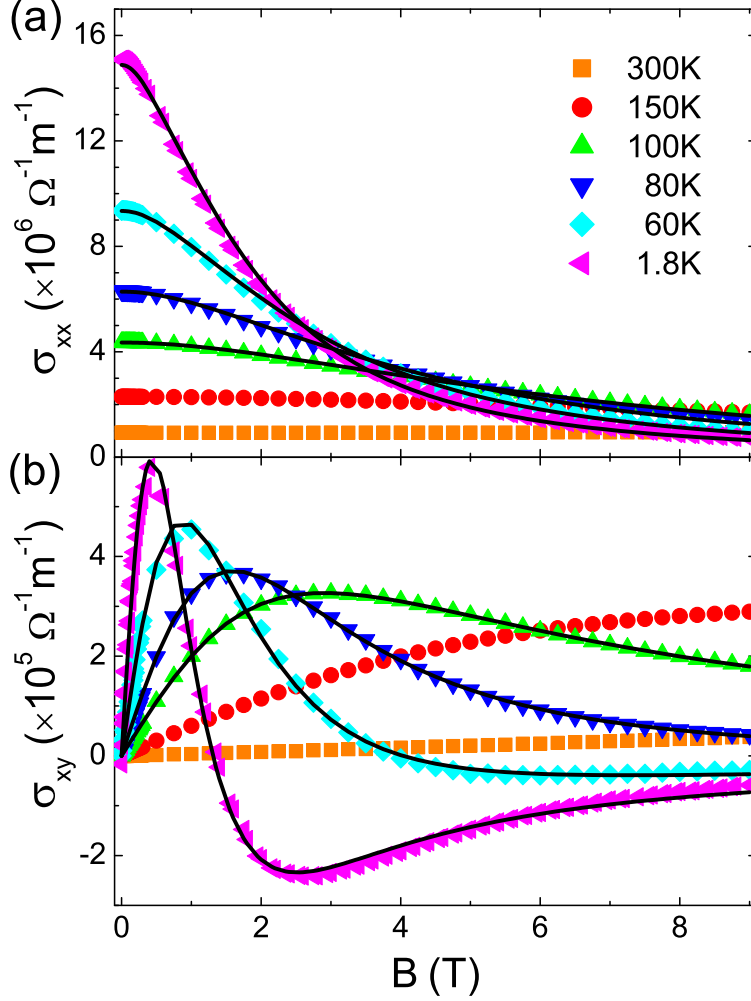


FIG. 7: (Color online) Field-dependence of the components of the magnetoconductivity tensor, σ_{xx} (a) and σ_{xy} (b). Black solid lines are fits of the curves using Eqs. (3,4) and a three-band model with two hole bands and one electron band.

IV. DISCUSSION

We should first show that the three-band picture that emerges from the above analysis of the magnetoresistance data is consistent with the DFT band structure calculations reported in Figure 9 in the vicinity of the Fermi level, ϵ_F . The bands crossing at ϵ_F and the Fermi sheets are as follows:

1. Two linearly dispersive bands cross ϵ_F almost exactly at mid-distance along the ΓM direction. This linear dispersion is in agreement with the observation of highly mobile h_2 holes. Due to their weak dispersion along k_z , these bands form a conic Fermi

RRR	7.9	15.8
n_e ($\times 10^{19}$ cm $^{-3}$)	8.20(8)	8.75(9)
n_{h1} ($\times 10^{19}$ cm $^{-3}$)	7.07(14)	7.4(4)
n_{h2} ($\times 10^{19}$ cm $^{-3}$)	0.92(16)	1.17(12)

TABLE I: Carrier densities of two BaNiS₂ single crystals obtained from the analysis of the temperature- and field-dependent longitudinal and transverse conductivities by using eqs. (3,4), as explained in the text. The reported value are mean values of the carrier densities obtained at different temperatures. Number in parentheses indicate standard deviations.

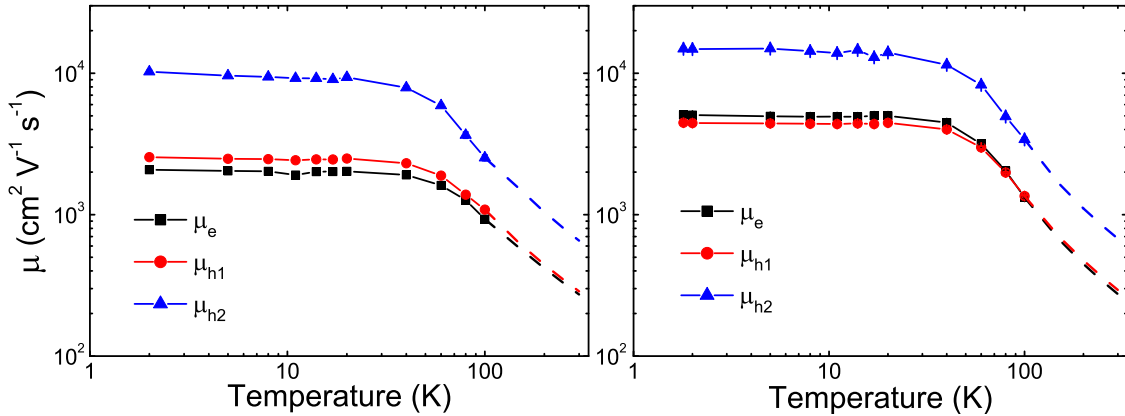


FIG. 8: (Color online) Carrier mobilities extracted from the analysis of the temperature and field dependence of the longitudinal and transverse conductivity for two BaNiS₂ samples with $RRR = 7.9$ (left panel) and $RRR = 15.8$ (right panel). The dashed lines above 100 K indicate the extrapolated behavior of the mobility by assuming a conventional $\mu_i \propto 1/T$ dependence expected for a metal with $\rho \propto T$.

surface similar to the Dirac cone in graphene. In the present case, contrary to the case of graphene, the shape of the cone basis in the k_x - k_y plane is not circular because of the different orbital character of the two bands that are mainly formed by $d_{3z^2-r^2}$ and $d_{x^2-y^2}$ states. In the light of the rich physics of the Dirac cones, it would be interesting to study the mobility of such h_2 holes as a function of doping.

2. The calculations predict a valence band and a conduction band at Γ and Z respectively. The two bands, split by spin-orbit coupling effects, form the two hole and

electron pockets visible along the Γ -Z direction, in agreement with the scenario of a second (h_1) hole band and of an electron band suggested by the previous analysis of magnetoresistance data.

3. In agreement with a very recent ARPES experiment⁷, two Rashba-split conduction bands are also visible at R . These bands touch the Fermi level and the volume of the resulting electron pockets is negligible as compared to that of the other pockets. Therefore, these bands should not affect the magnetotransport properties or marginally affect μ_e and n_e .

Second, we should discuss the anomalous properties that remain unexplained: (i) the levelling-off of the resistivity at values smaller than expected from the Mott-Ioffe-Regel limit; (ii) the crossover of resistivity regime at T^* and (iii) the linear temperature-dependence of the susceptibility above 100 K.

Typically, feature (i) is the signature of a resistivity saturation in the Mott-Ioffe-Regel limit described by the condition that the electron mean free path becomes comparable to the Fermi wave length. In 2D, this limit is reached for $\rho_{sat} = 2\pi\frac{e^2}{h}c \approx 2.2 \text{ m}\Omega\text{cm}$. In our case, $\rho_{ab}(400 \text{ K})$ is about one order of magnitude smaller than this value, so we consider the alternative explanation of a thermal activation of the carriers, which is significant in semimetals. Due to the low carrier density, n , which is apparent from the calculated density of states in Figure 9, this activation leads to a large relative increase of n , detected as a reduction of the resistivity coefficient at high temperatures, as observed in graphite at $\sim 80 \text{ K}$ ³². In BaNiS_2 , this reduction occurs at higher temperatures owing to the larger carrier density, $n \sim 10^{20} \text{ cm}^{-3}$, as compared to that of graphite, where $n \sim 10^{19} \text{ cm}^{-3}$ or less. This scenario is supported by the observation of a broad maximum of the thermoelectric power of BaNiS_2 at 175 K ¹. The ARPES band structure showing that the bottom of the Rashba-split bands barely touch the Fermi level further suggests that these are the bands populated by thermal activation. Magnetotransport measurements in high magnetic fields above 100 K may confirm the validity of this scenario.

As to the anomaly of the resistivity at T^* , we first consider a scenario of *umklapp* processes in combination with a singular DOS. It was previously proposed³³ that, under these conditions, the electronic scattering rate acquires a non-analytic contribution leading

to non-Fermi liquid transport properties down to very low temperatures. Specifically, the exponent of the temperature dependence of the resistivity can be significantly less than two³⁴. In the present case, the minimum of the Rashba-split bands at R indeed forms a van Hove singularity near ϵ_F . However, it is difficult to reconcile the large drop of the resistivity by a factor of two between T^* and 40 mK with the modest number of minority carriers associated with this singularity. As a second possibility, we recall that the linear behavior of the resistivity is characteristic of correlated metals, such as heavy fermions in the vicinity of an AF order³⁵ or superconducting cuprates^{36–38}. However, in these systems, the linear dependence extends to a much wider temperature range, whilst in the present case this dependence is rather similar to a crossover between conventional Bloch-Grüneisen regime above and low-temperature regime below T^* . Phenomenologically, this could be consistent with a crossover from a coherent Fermi-liquid regime to an incoherent regime controlled by a spin-freezing dynamics in the presence of a strong intra-atomic Hund coupling³⁹, which is expected in the present multiorbital case. According to this scenario, the loss of quasiparticle coherence at sufficiently high temperature leads to crossover of the transport regime⁴⁰ in qualitative agreement with the present data.

As to anomaly (iii), it is recalled that a similar anomaly has been reported on Fe-based pnictides⁴¹. For these systems, two scenarios have been proposed. The first scenario invokes the effect of the temperature-dependent chemical potential, μ , near a sharp peak of the DOS⁴². As apparent from the usual expression for the Pauli susceptibility:

$$\chi_{Pauli} = -\mu_B^2 \int_0^\infty D(\epsilon) \frac{\partial f(\epsilon, \mu, T)}{\partial \epsilon} d\epsilon \quad (5)$$

where $f(\epsilon, \mu, T)$ is the Fermi-Dirac distribution and μ_B is the Bohr magneton, a linear dependence of χ appears if the DOS strongly varies with energy near $\epsilon_F \approx \mu$, as in the case of semimetals. This simple picture has been proposed for pnictides on the basis of dynamic mean field theory (DMFT) calculations^{41,43}. At first sight, a similar picture may be applicable to the present case as well, for the calculated band structure of BaNiS₂ also exhibits a pronounced dip in the DOS at ~ 0.1 eV below ϵ_F . Indeed, the calculated $\chi(T)$ reproduce qualitatively the observed behavior of $\chi(T)$, including the existence of a tail at low temperature and the linear term at high temperatures. However, the experimental

slope $d\chi(T)/dT$ is about one order of magnitude larger than predicted using Eq. 5 and the calculated DOS. One may consider the possibility that the real DOS is much more singular than the calculated one due to renormalization effects. However, this possibility contrasts the evidence of modest renormalization effects from the present specific heat results and from ARPES measurements⁷.

A second scenario invokes the existence of short-range AF fluctuations^{23,24}, in agreement with previous theoretical studies of frustrated Heisenberg models with comparable nearest-neighbor and next-nearest-neighbor exchange coupling constants, J_1 and J_2 ⁴⁴. This scenario could be applicable to the present case since a J_1 - J_2 model is consistent with the observation of collinear AF order in BaCoS₂⁴⁵ and with the fact that the next-nearest-neighbor Ni-Ni distance in the square lattice of BaNiS₂ is only $\sqrt{2}$ times the nearest-neighbor distance. Thus, it is envisaged that residual short-range fluctuations may be present in BaNiS₂ as well. Suitable studies of spin dynamics would be required to probe directly these fluctuations.

V. CONCLUSION

In conclusion, the present study on high-quality BaNiS₂ single crystals suggests a consistent picture of compensated semimetal with two hole bands and one electron band, in agreement with ARPES data and DFT calculations. Notable is the high mobility of the minority holes attributed to a Dirac-like Fermi pocket, similar to the case of graphene. The transport properties are markedly two-dimensional and dominated by a conventional electron-phonon mechanism. While the low-temperature electronic specific heat is consistent with the calculated density of states, the magnetic susceptibility is strongly enhanced and exhibits a pronounced linear term at high temperature. This anomaly could be explained either by a strong variation of the density of state at ϵ_F , not predicted by DFT calculations, or by the presence of short-range AF fluctuations reminiscent of the AF order observed in BaCoS₂. A further signature of unconventional behavior is a striking crossover of the resistivity from a conventional Bloch-Grüneisen behavior to a linear behavior below $T^* \sim 6$ K. We envisage that this crossover may reflect the loss of quasi-particle coherence caused by a spin-freezing dynamics in presence of a large Hund coupling. Further studies are required to verify the validity of the above scenario according to which both intra- and inter-atomic magnetic interactions strongly alter the stability of a conventional Fermi-liquid ground state.

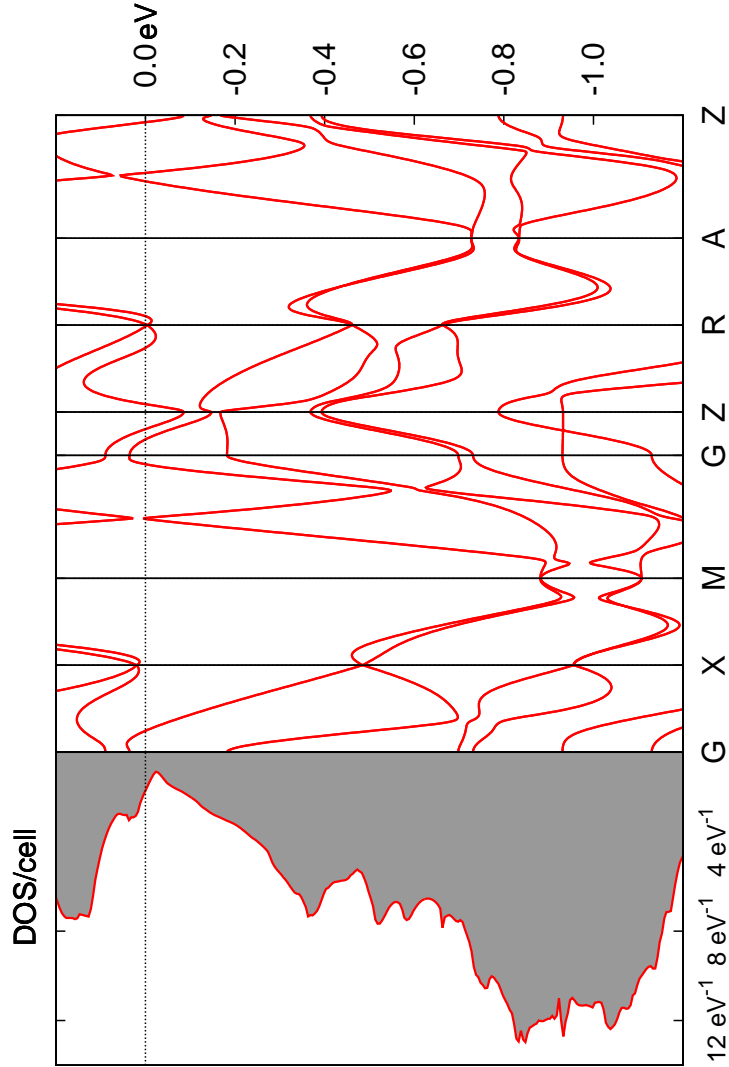


FIG. 9: (Color online) Calculated electronic bands and total density of states. The dotted line indicates the Fermi level, ϵ_F .

Acknowledgments

This work was partly supported by the University Pierre and Marie Curie under the *Programme émergence* funding program and by the IDRIS/GENCI computational resources under the project No. 096493. We are grateful to B. Léridon and R. Lobo for giving us access to the VSM-SQUID apparatus of their laboratory supported by the *Région Île-de-France*.

We are thankful to J. Biscaras for fruitful discussions.

* david.santos-cottin@espci.fr

† yannick.klein@upmc.fr

¹ J. Takeda, K. Kodama, H. Harashima, and M. Sato, *J. Phys. Soc. Jpn.* **63**, 3564 (1994), URL <http://jpsj.ipap.jp/link?JPSJ/63/3564/>.

² M. Imada, A. Fujimori, and Y. Tokura, *Rev. Mod. Phys.* **70**, 1039 (1998), URL <http://link.aps.org/doi/10.1103/RevModPhys.70.1039>.

³ D. C. Johnston, *Advances in Physics* **59**, 803 (2010), <http://dx.doi.org/10.1080/00018732.2010.513480>, URL <http://dx.doi.org/10.1080/00018732.2010.513480>.

⁴ R. Joynt and L. Taillefer, *Rev. Mod. Phys.* **74**, 235 (2002), URL <http://link.aps.org/doi/10.1103/RevModPhys.74.235>.

⁵ K. Kodama, H. Fujishita, H. Harashina, S. Taniguchi, J. Takeda, and M. Sato, *J. Phys. Soc. Jpn.* **64**, 2069 (1995), URL <http://jpsj.ipap.jp/link?JPSJ/64/2069/>.

⁶ P. A. Lee, N. Nagaosa, and X.-G. Wen, *Rev. Mod. Phys.* **78**, 17 (2006), URL <http://link.aps.org/doi/10.1103/RevModPhys.78.17>.

⁷ D. Santos-Cottin, M. Casula, G. Lantz, Y. Klein, L. Petaccia, P. Lefèvre, F. Bertrand, E. Papalazarou, M. Marsi, and A. Gauzzi, *Nat. Commun.* to be published (2016).

⁸ S. Shamoto, S. Tanaka, E. Ueda, and M. Sato, *J. Cryst. Growth* **154**, 197 (1995), ISSN 0022-0248, URL <http://www.sciencedirect.com/science/article/pii/0022024895002251>.

⁹ I. E. Grey and H. Steinfink, *J. Am. Chem. Soc.* **92**, 5093 (1970), <http://pubs.acs.org/doi/pdf/10.1021/ja00720a015>, URL <http://pubs.acs.org/doi/abs/10.1021/ja00720a015>.

¹⁰ L. J. van der Pauw, *Philips Res. Repts.* **13**, 1 (1958).

¹¹ X. F. Wang, T. Wu, G. Wu, R. H. Liu, H. Chen, Y. L. Xie, and X. H. Chen, *New Journal of Physics* **11**, 045003 (2009), URL <http://stacks.iop.org/1367-2630/11/i=4/a=045003>.

¹² J. P. Perdew, K. Burke, and M. Ernzerhof, *Phys. Rev. Lett.* **77**, 3865 (1996), URL <http://link.aps.org/doi/10.1103/PhysRevLett.77.3865>.

¹³ P. Giannozzi, S. Baroni, N. Bonini, M. Calandra, R. Car, C. Cavazzoni, D. Ceresoli, G. L. Chiarotti, M. Cococcioni, I. Dabo, et al., *J. Phys.: Condens. Matter* **21**, 395502 (19pp) (2009),

URL <http://www.quantum-espresso.org>.

- ¹⁴ R. Gebauer and S. Baroni, Phys. Rev. B **61**, R6459 (2000), URL <http://link.aps.org/doi/10.1103/PhysRevB.61.R6459>.
- ¹⁵ A. D. Corso and A. M. Conte, Phys. Rev. B **71**, 115106 (2005), URL <http://link.aps.org/doi/10.1103/PhysRevB.71.115106>.
- ¹⁶ P. E. Blöchl, O. Jepsen, and O. K. Andersen, Phys. Rev. B **49**, 16223 (1994), URL <http://link.aps.org/doi/10.1103/PhysRevB.49.16223>.
- ¹⁷ J. Takeda, Y. Yasui, H. Sasaki, and M. Sato, Journal of the Physical Society of Japan **66**, 1718 (1997), <http://dx.doi.org/10.1143/JPSJ.66.1718>, URL <http://dx.doi.org/10.1143/JPSJ.66.1718>.
- ¹⁸ J. Takeda, Y. Kobayashi, K. Kodama, H. Harashina, and M. Sato, J. Phys. Soc. Jpn. **64**, 2550 (1995), URL <http://jpsj.ipap.jp/link?JPSJ/64/2550/>.
- ¹⁹ L. Matheiss, Solid State Com. **93**, 879 (1995), ISSN 0038-1098, URL <http://www.sciencedirect.com/science/article/pii/0038109894009007>.
- ²⁰ I. Hase, N. Shirakawa, and Y. Nishihara, J. Phys. Soc. Jpn. **64**, 2533 (1995), URL <http://jpsj.ipap.jp/link?JPSJ/64/2533/>.
- ²¹ H. Kuriyaki, K. Tokunaga, S. Nishiyoka, and K. Hirakawa, J. Phys. IV France **3**, 277 (1993), URL <http://dx.doi.org/10.1051/jp4:1993256>.
- ²² L. S. Martinson, J. W. Schweitzer, and N. C. Baenziger, Phys. Rev. B **54**, 11265 (1996), URL <http://link.aps.org/doi/10.1103/PhysRevB.54.11265>.
- ²³ R. Klingeler, N. Leps, I. Hellmann, A. Popa, U. Stockert, C. Hess, V. Kataev, H.-J. Grafe, F. Hammerath, G. Lang, et al., Phys. Rev. B **81**, 024506 (2010), URL <http://link.aps.org/doi/10.1103/PhysRevB.81.024506>.
- ²⁴ X. F. Wang, T. Wu, G. Wu, H. Chen, Y. L. Xie, J. J. Ying, Y. J. Yan, R. H. Liu, and X. H. Chen, Phys. Rev. Lett. **102**, 117005 (2009), URL <http://link.aps.org/doi/10.1103/PhysRevLett.102.117005>.
- ²⁵ A. Bid, A. Bora, and A. K. Raychaudhuri, Phys. Rev. B **74**, 035426 (2006), URL <http://link.aps.org/doi/10.1103/PhysRevB.74.035426>.
- ²⁶ Y. Maeno, H. Hashimoto, K. Yoshida, S. Nishizaki, T. Fujita, J. G. Bednorz, and F. Lichtenberg, Nature **372**, 532 (1994), URL <http://www.nature.com/nature/journal/v372/n6506/pdf/372532a0.pdf>.

- ²⁷ V. Zverev and D. Shovkun, Phys. C: Supercond **391**, 315 (2003), ISSN 0921-4534, URL <http://www.sciencedirect.com/science/article/pii/S0921453403009572>.
- ²⁸ Y. Ishiwata, Y. Shiomi, J. S. Lee, M. S. Bahramy, T. Suzuki, M. Uchida, R. Arita, Y. Taguchi, and Y. Tokura, Nat. Mater. **12**, 512 (2013), URL <http://dx.doi.org/10.1038/nmat3621>.
- ²⁹ P. Kapitza, Proceedings of the Royal Society of London A: Mathematical, Physical and Engineering Sciences **119**, 358 (1928), ISSN 0950-1207.
- ³⁰ M. Kohler, Ann. Phys. **424**, 211 (1938), ISSN 1521-3889, URL <http://onlinelibrary.wiley.com/doi/10.1002/andp.19384240124/abstract>.
- ³¹ D. L. Rode, *Low Field Electron Transport*, vol. 10 of *Semiconductors and Semimetals* (Academic Press, New York, 1975), ISBN 9780127521114.
- ³² Y. Hishiyama and Y. Kaburagi, Carbon **30**, 483 (1992), ISSN 0008-6223, URL <http://www.sciencedirect.com/science/article/pii/000862239290047Z>.
- ³³ J. M. Buhmann, Phys. Rev. B **88**, 245128 (2013), URL <http://link.aps.org/doi/10.1103/PhysRevB.88.245128>.
- ³⁴ S. Schmitt, Phys. Rev. B **82**, 155126 (2010), URL <http://link.aps.org/doi/10.1103/PhysRevB.82.155126>.
- ³⁵ G. R. Stewart, Rev. Mod. Phys. **73**, 797 (2001), URL <http://link.aps.org/doi/10.1103/RevModPhys.73.797>.
- ³⁶ R. A. Cooper, Y. Wang, B. Vignolle, O. J. Lipscombe, S. M. Hayden, Y. Tanabe, T. Adachi, Y. Koike, M. Nohara, H. Takagi, et al., Science **323**, 603 (2009), <http://www.sciencemag.org/content/323/5914/603.full.pdf>, URL <http://www.sciencemag.org/content/323/5914/603.abstract>.
- ³⁷ N. E. Hussey, R. A. Cooper, X. Xu, Y. Wang, I. Mouzopoulou, B. Vignolle, and C. Proust, Philosophical Transactions of the Royal Society A: Mathematical, Physical and Engineering Sciences **369**, 1626 (2011), <http://rsta.royalsocietypublishing.org/content/369/1941/1626.full.pdf+html>, URL <http://rsta.royalsocietypublishing.org/content/369/1941/1626.abstract>.
- ³⁸ Y. Ando, S. Komiya, K. Segawa, S. Ono, and Y. Kurita, Phys. Rev. Lett. **93**, 267001 (2004), URL <http://link.aps.org/doi/10.1103/PhysRevLett.93.267001>.
- ³⁹ P. Werner, E. Gull, M. Troyer, and A. J. Millis, Phys. Rev. Lett. **101**, 166405 (2008), URL <http://link.aps.org/doi/10.1103/PhysRevLett.101.166405>.
- ⁴⁰ A. Georges, L. de' Medici, and J. Mravlje, Annual Review of Condensed Matter

- Physics **4**, 137 (2013), <http://dx.doi.org/10.1146/annurev-conmatphys-020911-125045>, URL <http://dx.doi.org/10.1146/annurev-conmatphys-020911-125045>.
- ⁴¹ S. L. Skornyakov, A. A. Katanin, and V. I. Anisimov, Phys. Rev. Lett. **106**, 047007 (2011), URL <http://link.aps.org/doi/10.1103/PhysRevLett.106.047007>.
- ⁴² B. Sales, M. McGuire, A. Sefat, and D. Mandrus, Phys. C: Supercond. **470**, 304 (2010), ISSN 0921-4534, URL <http://www.sciencedirect.com/science/article/pii/S0921453410000651>.
- ⁴³ S. L. Skornyakov, V. I. Anisimov, and D. Vollhardt, Phys. Rev. B **86**, 125124 (2012), URL <http://link.aps.org/doi/10.1103/PhysRevB.86.125124>.
- ⁴⁴ F. Mila, D. Poilblanc, and C. Bruder, Phys. Rev. B **43**, 7891 (1991), URL <http://link.aps.org/doi/10.1103/PhysRevB.43.7891>.
- ⁴⁵ D. Mandrus, J. L. Sarrao, B. C. Chakoumakos, J. A. Fernandez-Baca, S. E. Nagler, and B. C. Sales, Journal of Applied Physics **81**, 4620 (1997), URL <http://scitation.aip.org/content/aip/journal/jap/81/8/10.1063/1.365182>.